

Microscopic Theory of the Single Impurity Surface Kondo Resonance

Chiung-Yuan Lin,¹ A. H. Castro Neto,¹ and B. A. Jones²

¹*Department of Physics, Boston University, 590 Commonwealth Ave., Boston, MA 02215*

²*IBM Almaden Research Center, San Jose, CA 95120-6099*

(Dated: 22nd March 2022)

We develop a microscopic theory of the single impurity Kondo effect on a metallic surface. We calculate the hybridization energies for the Anderson Hamiltonian of a magnetic impurity interacting with surface and bulk states and show that, contrary to the Kondo effect of an impurity in the bulk, the hybridization matrix elements are strongly dependent on the momentum around the Fermi surface. Furthermore, by calculating the tunneling conductance of a scanning tunneling microscope (STM), we show that when the magnetic impurity is located at a surface the Kondo effect can occur with equal strength between bulk and surface states. We compare our results with recent experiments of Co impurities in Cu(111) and Cu(100) surfaces and find good quantitative agreement.

PACS numbers: 72.15.Qm, 68.37.Ef, 72.10.Fk

I. INTRODUCTION

When a magnetic impurity is located in the bulk of a metal it undergoes a non-trivial many-body scattering with the electronic states at the Fermi energy, ϵ_F , called the Kondo effect¹. The bulk Kondo effect (to be contrasted with the surface Kondo effect studied in this paper) is one of the best studied problems in condensed matter physics and many different techniques from renormalization group² to Bethe ansatz³ have been used over the years. The basic mechanism of the Kondo effect is the magnetic screening of the impurity (the formation of the Kondo singlet) at temperatures T below the Kondo temperature T_K . Above T_K the magnetic impurity behaves paramagnetically but for $T < T_K$ a resonance is formed close to the Fermi surface. The Kondo effect is very important in modern condensed matter theory and appears in many different areas of research, from U and Ce intermetallics (heavy-fermions)⁴ to quantum dots⁵. There is a wide variety of phenomena that can be described within the universality of the Kondo problem. The Kondo effect can be observed experimentally in measurements of the temperature dependence of resistivity (the so-called resistivity minimum)⁶, and also in thermodynamic measurements such as specific heat and magnetic susceptibility⁴ of dilute magnetic alloys, due to the enhancement of the density of states close to the Fermi energy (the Abrikosov-Suhl resonance⁷). The enhancement of the density of states is related to the change of the characteristic energy scales from ϵ_F to $k_B T_K$ and therefore in the density of states from $N(0) \propto 1/\epsilon_F$ to $N^*(0) \propto 1/(k_B T_K) \gg N(0)$ since $\epsilon_F \gg k_B T_K$.

The Kondo effect was also observed recently in STM studies of magnetic atoms on metallic surfaces^{8,9,10} (see Fig.1). In a STM experiment electrons from a sharp tip tunnel into the material to be studied, creating a tunneling current I due to the application of a potential V . Roughly speaking a STM experiment measures the local density of states at the Fermi energy via the differential tunneling conductance dI/dV ¹¹. When a STM

tip is away from the magnetic impurity it measures the substrate density of states, $N(0)$; however, close to the impurity (that we call the adatom) electrons from the tip can tunnel directly to the impurity. The theory of STM is far from trivial because electrons from the tip not only tunnel to the adatom but also to the bulk and surface states, that is, there are various different channels of tunneling that lead to interference effects that have to be taken into consideration for the proper interpretation of the experimental data.

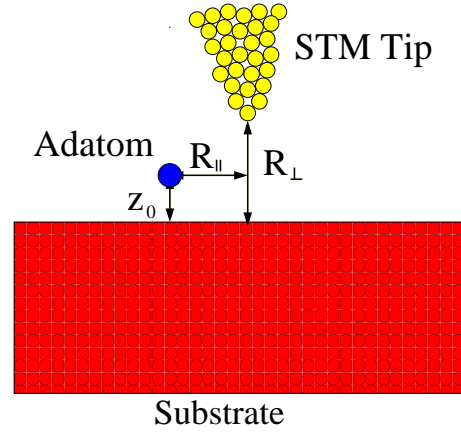


Figure 1: Schematic picture of a STM measurement: z_0 is the distance of the adatom to the surface, R_\perp is the distance of the STM tip from the surface, and R_\parallel is the distance, along the surface, between the STM tip and the adatom.

The basic starting point for the study of the Kondo effect is the Anderson impurity Hamiltonian¹²:

$$H_s = \sum_a \left(\epsilon_a \sum_\sigma c_{a\sigma}^\dagger c_{a\sigma} + U n_{a\uparrow} n_{a\downarrow} \right) + \sum_{\mathbf{k}\sigma} \epsilon_{\mathbf{k}} c_{\mathbf{k}\sigma}^\dagger c_{\mathbf{k}\sigma} + \sum_{\mathbf{k},\sigma,a} t_{\mathbf{k}a} \left(c_{\mathbf{k}\sigma}^\dagger c_{a\sigma} + \text{H.c.} \right), \quad (1)$$

where $c_{a\sigma}$ ($c_{a\sigma}^\dagger$) is the annihilation (creation) operator for an electron on a localized atomic state (impurity state)

with angular momentum labelled by a , energy ϵ_a and spin σ ($\sigma = \uparrow, \downarrow$), $c_{\mathbf{k}\sigma}$ ($c_{\mathbf{k}\sigma}^\dagger$) is the annihilation (creation) operator for an electron on the conduction band with dispersion ϵ_k and momentum \mathbf{k} , $n_{a\sigma} = c_{a\sigma}^\dagger c_{a\sigma}$ is the number operator of the impurity state, and $t_{\mathbf{k}a}$ is the hybridization energy between the impurity and conduction states (the electron operators obey anti-commutation rules: $\{c_a, c_b^\dagger\} = \delta_{a,b}$).

One of the characteristics of the Anderson impurity model is the distinction between substrate and adatom wavefunctions. Although most theoretical works do not question the distinction made *a priori* between these quantum states, it turns out that this distinction is not completely natural. The reason is very simple: when an impurity atom is introduced in a metal, it hybridizes with the metallic states losing its identity. However, it leaves behind a phase shift $\delta_{\mathbf{k}}$ in the original metallic states. Thus, the impurity state cannot be really distinguished from the host states from the quantum mechanical point of view. Nevertheless, Anderson¹² makes the point that because the d-orbitals are a inner shell, the Coulomb energy U for double occupancy of those orbitals is large and they must be distinguished from metallic states where the Coulomb energy is strongly suppressed by screening effects. Thus, the distinction between these two types of states can only be clearly made when these states are orthogonal to each other so that the impurity does not cause a direct perturbation in the substrate spectrum. Nevertheless, even in metals where the electronic bands are generated out of d-orbitals (as in the case of Cu), the strong metallic bonding leads to a large s-wave character of the bands and to very small overlap with the adatom d-orbitals (that is, these states are “naturally” orthogonal¹³). Nevertheless, this orthogonality can only be distinguished *a posteriori*. In fact, we have found, by direct numerical computation, that this is the case in the surface Kondo effect. Finally, as pointed out by Anderson¹² (see also ref.¹⁴), the orthogonality of these states is not fundamental for the magnetic phenomenon which is essentially a local effect and all the subtleties associated with orthogonality become encapsulated into the hybridization matrix elements $t_{\mathbf{k}a}$ which become a phenomenological parameter to be obtained indirectly from the experiment. However, in trying to understand the STM experiments, and especially the role played by the surface and bulk states, we cannot simply take these matrix elements as phenomenological parameters since we would not be able to separate the contributions coming from the bulk and the surface of the Cu substrate.

Hence, in this paper we follow the scheme proposed by Tsvelik and Wiegmann¹⁴ and work with non-orthogonalized states. In this case the hybridization energies are given by:

$$t_{\mathbf{k}a} = (\epsilon_k + \epsilon_a) \int d^3r \psi_a^*(\mathbf{r}) \psi_{\mathbf{k}}(\mathbf{r}) \quad (2)$$

where $\psi_a(\mathbf{r})$ is the atomic state of the impurity which is localized on the impurity site (that is, it decays ex-

ponentially away from the impurity) and $\psi_{\mathbf{k}}(\mathbf{r})$ is the Bloch wavefunction of the crystal. The hybridization energy depends not only on the amplitude but also on the direction of \mathbf{k} . Nevertheless, it is usually assumed that the hybridization is constant in momentum space, that is, $t_{\mathbf{k},a} = t$. Although this assumption maybe warranted for spherical gapless Fermi surfaces (since the momentum dependence “averages out” and most of the interesting physics occurs at the Fermi surface) it is not valid for metals where the chemical potential crosses gaps in the electronic spectrum. The Kondo Hamiltonian can be obtained from (1) in the limit of $|t| \ll \epsilon_a, U$ via the Schrieffer-Wolf transformation¹⁵ that maps the Hamiltonian (1) onto:

$$H_K = \sum_{\mathbf{k}\sigma} \epsilon_k c_{\mathbf{k}\sigma}^\dagger c_{\mathbf{k}\sigma} + J_K \mathbf{S} \cdot \mathbf{s}(0) \quad (3)$$

where \mathbf{S} is the impurity spin, $s^a(0) = \hbar/2 \sum_{\mathbf{k}, \mathbf{k}', \alpha, \beta} c_{\mathbf{k}\alpha}^\dagger \sigma_{\alpha, \beta}^a c_{\mathbf{k}'\beta}$ is the electron spin at the impurity site (σ^a with $a = x, y, z$ are Pauli matrices) and

$$J_K \approx |t|^2 \left(\frac{1}{|\epsilon_a|} + \frac{1}{|\epsilon_a + U|} \right) \quad (4)$$

is the exchange interaction between local spins and conduction electrons (the energy is measured relative to the Fermi energy). In going from (1) to (3) we have disregarded a series of physical processes that cannot be described as spin exchange interactions, foremost being the variable occupancy of the impurity site.

Even simple metals like Cu have energy gaps in their electronic spectrum due to the periodic potential generated by the Cu ions^{16,17}. For instance, it is well-known that for Cu along the (111) direction there is a gap of 5.1 eV at the Fermi energy while there are no gaps along the (100) direction (see Fig.2). On the one hand, $t_{\mathbf{k}a}$ does not exist for bulk states when \mathbf{k} points along the (111) direction. However, because of the bulk gap, one has a surface state in the Cu(111) surface¹⁸ (a state that decays exponentially in the (111) direction but it is extended in the directions perpendicular to (111)) that can hybridize with the impurity located on the Cu(111) surface. On the other hand, there are no surface states in the (100) direction to hybridize with an impurity located on the Cu(100) surface, although bulk states hybridize with it since their wavefunctions decay exponentially outside of the crystal. Previous studies¹⁹ on the surface Kondo effect either assume a momentum-independent hybridization $t_{\mathbf{k}a}$ or sum average over a gapless Fermi surface¹¹. By ignoring momentum dependence or the gap structure of the Fermi surface, the comparison between Cu(111) and Cu(100) surface Kondo effects of noble metals is not possible. In fact, we show that recent STM experiments of atoms located in the Cu(111) and Cu(100) surfaces have been interpreted incorrectly because of these differences. In particular, we show that the surface Kondo effect between a magnetic atom located on the Cu(111)

surface and the Cu(111) surface state is quantitatively similar to the surface Kondo effect of a magnetic atom on a Cu(100) surface with bulk states. The main reason for this similarity comes from the fact that the bulk state that dominates the Kondo scattering is the one with the largest penetration in the work-function barrier, that is, the state with momentum perpendicular to the Cu(100) surface. The state with momentum perpendicular to the Cu(100) surface has essentially the same decay rate out of the crystal as the surface state in the Cu(111) surface and therefore similar hybridization with the magnetic impurity.

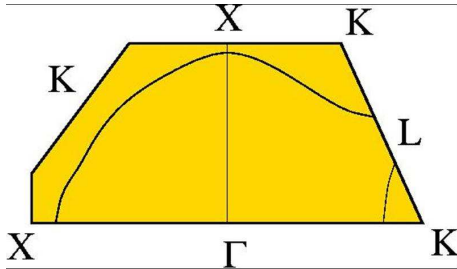


Figure 2: Planar cut of the bulk Cu Fermi surface in the first Brillouin zone: Γ -L is the (111) direction (notice the absence of states due to the bulk gap); Γ -X is the (100) direction.

In the presence of the tip new terms have to be added to the Hamiltonian (1) that describe the tunneling processes of tip-to-atom and tip-to-substrate¹¹. The tunneling processes of tip-to-atom is given by:

$$H_{at} = \sum_{\sigma,a} t_{ap} (c_{a\sigma}^\dagger c_{p\sigma} + \text{H.c.}). \quad (5)$$

where $c_{p\sigma}$ ($c_{p\sigma}^\dagger$) annihilates (creates) an electron at the tip and t_{ap} is the hybridization energy between tip and atom. The tip-to-substrate hybridization is given by:

$$H_t = \sum_{k\sigma} t_{kp} (c_{k\sigma}^\dagger c_{p\sigma} + \text{H.c.}), \quad (6)$$

where t_{kp} is the hybridization energy between substrate (bulk or surface state) and atom. The tip Hamiltonian is simply

$$H_{st} = \sum_{\sigma} \epsilon_p c_{p\sigma}^\dagger c_{p\sigma} \quad (7)$$

where ϵ_p is the energy of the electron states on the tip. The total Hamiltonian of the tip-substrate-adsorbate system is $H = H_s + H_t + H_{at} + H_{st}$. As in the case of (1) the hybridization energies are given by:

$$t_{\alpha\beta} = (\epsilon_\alpha + \epsilon_\beta) \int d^3r \psi_\alpha^*(\mathbf{r}) \psi_\beta(\mathbf{r}) \quad (8)$$

with $\alpha, \beta = \mathbf{k}, a, p$ labeling the wavefunctions, $\psi_\alpha(\mathbf{r})$, for substrate, atom and tip, respectively. Notice that the

complexity in this problem comes from the interference between the different channels of tunneling.

In the present work, we will consider the case of Co on Cu surfaces while our theory is applicable to any magnetic adatom on noble metal surfaces. Our main objectives are: (i) the calculation of the hybridization matrix elements between the different wavefunctions in the problem (bulk, surface, impurity, and STM tip) with the smallest number of adjustable parameters, and (ii) the description of the surface Kondo effect via STM measurements. While the spectrum of bulk and surface states is readily available in the literature, very little has been published on the actual form of the states. Instead of embarking on a complicated calculation of wavefunctions via heavy numerical techniques, we opted for a simpler approach that can provide quantitative results that can be directly compared to the experiment as well as intuitive understanding of the problem. As we are going to show, our simplified models have limitations in explaining some of the available STM data and more detailed work is required. We hope our work stimulates other works that make use of more sophisticated methods to calculate the matrix elements because, as we are going to show, they are fundamental for the understanding of magnetism in metallic surfaces. We model the periodic potential inside of the crystal in the nearly-free electron approximation and obtain the bulk gaps as observed in metallic Cu. The surface states are obtained after the modeling of the surface potential in terms of the image charge in the vacuum. The energies of surface states and resonances in each surface are in very good agreement with photoemission results in Cu(111) and Cu(100) surfaces. Following the literature in STM theory, the impurity is modeled via standard Hydrogen-like wave functions.

The paper is organized as follows: In Sec. II, we model the ionic potentials that give rise to the wavefunctions of the metallic host, atom, and the STM tip. Using the wavefunctions and their spectrum we discuss the Cu band structure, both the bulk and Cu(111) surface state. In Sec. III we present the results for the hybridization matrix elements that determine the hybridization energies as a function of the distance from the surface and atom and also as a function of the momentum. The surface Kondo effect is discussed in Sec. IV in the context of the Schrieffer-Wolf transformation and the slave-boson mean-field theory. Using the calculated hybridization energies the differential conductance is calculated in Sec. V and compared with the STM data. Sec. VI contains our conclusions.

II. WAVEFUNCTIONS AND SPECTRUM

In this section, we obtain wavefunctions needed to calculate the tunneling matrix elements (8). This is the first step towards the STM differential conductance. As discussed in the introduction we are going to use simple models for the various potentials involved in the problem

so that we can make analytical progress in calculating the hybridization energies.

Metallic Cu is a very good metal with a nearly spherical Fermi surface except for the gaps in the (111) direction. These gaps have their origin in the periodic potential generated by the ions (see Fig. 2). Although the Cu states can be obtained from first principle calculations¹⁶ we adopt the nearly free electron approximation and model the bulk potential with a simple periodic function. Furthermore, in order to study the surface states we consider a semi-infinite crystal where the bulk is located at $z < 0$ (see Fig. 3). We write the potential in the substrate as:

$$V(\mathbf{r}) = \begin{cases} -2V_1 \cos \frac{2\pi z}{a} & , \text{ for } z < 0, \\ -2V_1 & , \text{ for } 0 < z < z_1, \\ V_0 - \frac{e^2}{4(z-z_{\text{im}})} & , \text{ for } z > z_1, \end{cases} \quad (9)$$

where V_1 is the bulk potential, a is the lattice spacing in the direction of the surface, V_0 is the work function measured from the bottom of the conduction band, z_{im} is the image plane, chosen in such a way that the image potential joins the constant potential $-2V_1$ continuously, and is related to z_1 as

$$z_{\text{im}} = z_1 - \frac{e^2}{4(V_0 + 2V_1)}. \quad (10)$$

In the potential Eq. (9), z_1 is the only free parameter. The eigenfunctions and eigenenergies for the Schrödinger equation associated with the potential (9) can be calculated exactly and the details are given in Appendix A.

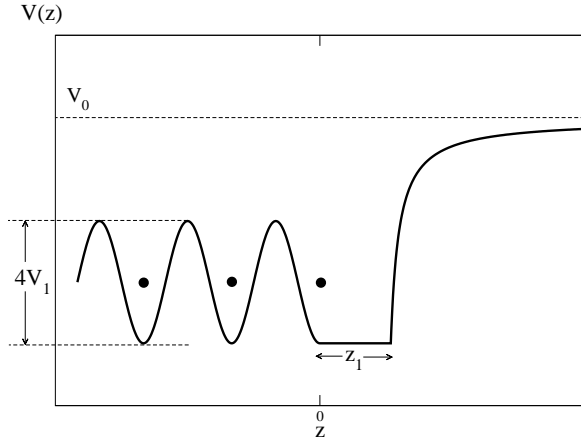


Figure 3: Plot of the image potential energy near a crystal surface. The solid dots are crystal atoms.

Let us consider first the case of the (111) direction. In order to fit the experimental band structure¹⁷ along the (111) direction in the nearly-free-electron potential we find that $V_1 = 2.55$ eV, $V_0 = 13.55$ eV. These values

provide a very good description of the band gap in the (111) direction and also of the ionization energy of metallic Cu. The Cu(111) surface has a band of surface states as measured by photoemission, starting 390 meV below the Fermi surface^{17,20}. By solving the Schrödinger problem for the potential (9) we find the surface band (see Appendix A) and fix the value of $z_1 = 1.66 \text{ \AA}$ in order to fit the photoemission results. Using this value for z_1 , we also obtain the next surface state at 788 meV below the vacuum level. This result agrees well with photoemission experiments that find the second surface state at 830 meV below the vacuum level²¹. Thus, we were able to get a consistent description of two independent experiments with a single fitting parameter. In Fig. 4 we show a plot of the surface state wavefunction as a function of the distance away from the surface (the wavefunction is chosen to be a real function). Notice the slow decay of this state inside the crystal in the direction perpendicular to the surface.

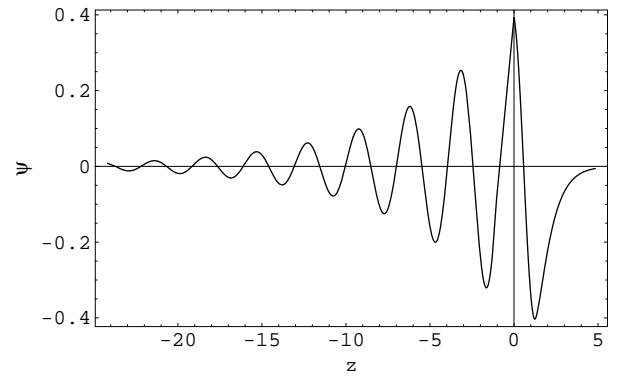


Figure 4: The Cu(111) surface state with energy 0.39 eV below the Fermi surface. The vertical axis represents its normalized wavefunction multiplied by the box size L . The horizontal axis represents z in \AA .

In the 3-dimensional k -space of Cu, a gaped “cavity” is centered around the (111) direction near the Fermi level and has the bulk band surrounding this gaped region²². By decomposing the momentum of a bulk state \mathbf{k} into \mathbf{k}_\perp (perpendicular to the surface) and \mathbf{k}_\parallel (parallel to the surface), one expects that the larger k_\perp , the larger wavefunction tail outside the crystal, which makes a significant difference on their contributions to the surface Kondo effect. As a result, it is important to carefully exclude the (111) gaped region from the Fermi sphere when calculating the surface Kondo effect.

It is known that a nearly-free-electron band has a parabolic dispersion not too close to the band edge, where “band edge” refers to the interface between the bulk band and the gap in the 3D k -space. When calculating the STM tunneling conductance, one would have to include the contribution close to the band edge as well. However, the band-edge contribution is typically much smaller than the one coming from the parabolic band, so

we can take merely the contribution from the parabolic band. For the Cu(111) band, we terminate the parabolic band 0.7 eV below the band edge. As long as we work in a parabolic band, the bulk-state wavefunction inside the crystal takes a plane-wave form.

We now turn to the case of the (100) direction. We find that we get good agreement with band structure calculations¹⁷ by choosing $V_1 = 3.05$ eV, and $V_0 = 13.45$ eV. In contrast to the (111) direction, the (100) direction has no true surface state near the Fermi surface. However, there is a surface resonance at 1.15 eV above the Fermi level²³ that can be well described by choosing $z_1 = 1.51$ Å. When calculating the tunneling conductance, we can safely sum over the entire Fermi sphere and adopt a parabolic dispersion, i.e. a plane-wave wavefunction inside the crystal.

It is the d-orbital of the adatom that actually participates in the Kondo resonance. When one of these atoms is placed on a metal surface, its outmost s-wave electrons either get transferred to the metal conduction band or to its own d-orbital. For example, the Co adatom tends to form $[\text{Ar}]3d^9$ on a Cu surface¹⁹ and therefore has an effective spin 1/2. As a result, an adatom d-wavefunction can be modeled as a Hydrogen atom with an effective charge Z_{eff} given by:

$$\psi_a(\mathbf{r}) = R_{n2}(Z_{\text{eff}}, r)Y_{2m}(\theta, \phi), \quad (11)$$

where $Y_{2m}(\theta, \phi)$ are Spherical Harmonics and R_{n2} are Hydrogen radial wavefunctions. The effective charge Z_{eff} can be determined by comparing r_{max} , defined by,

$$\left. \frac{d|\psi_a|^2}{dr} \right|_{r=r_{\text{max}}} = 0, \quad (12)$$

with the experimentally observed d-orbital radius for metallic Co, $r_{\text{max}} = 1.25$ Å. In our calculation we orient the axis of quantization for the atomic problem along the direction perpendicular to the surface.

The STM tip wavefunction is modeled following Tersoff and Hamann²⁴ who proposed a wavefunction of the form:

$$\psi_p = \begin{cases} Re^{\kappa R} \frac{\exp(-\kappa r)}{r}, & \text{for } r > R, \\ 1, & \text{for } r < R, \end{cases} \quad (13)$$

where R is the radius of curvature of the tip about its center, the decay constant $\kappa = \sqrt{2m_t^*(\phi - \epsilon_p)}$ controls the wavefunction tail, and ϕ is the tip work function. Notice that the adatom and tip wavefunctions are normalizable, that is, $\int d^3r |\psi_a(\mathbf{r})|^2 = \int d^3r |\psi_p(\mathbf{r})|^2 = 1$, when integrated over the entire space.

The set of three different wavefunctions (substrate, adatom, and tip) are the main elements required for the calculation of the hybridization energies in the Anderson impurity Hamiltonian.

III. HYBRIDIZATION ENERGIES

Using the results of Eq.(A1), (11) and (13) we can evaluate the overlap integrals in (8) that are important for the

hybridization energies. Let us first remark that the normalization of each of these wavefunctions is different; for instance, the bulk state is normalized in a box of size L^3 , where L is one of the dimensions of the box. The surface state, however, since it decays exponentially away from the surface but is extended on the surface, is normalized in an area of size L^2 . Finally, the adatom and tip states always decay exponentially and therefore do not require any box normalization. Thus, it is convenient to redefine the wavefunctions so that:

$$\begin{aligned} \psi_{B,\mathbf{k}}(\mathbf{r}) &= \frac{1}{L^{3/2}} \phi_{3,\mathbf{k}}(\mathbf{r}) \\ \psi_{S,\mathbf{k}}(\mathbf{r}) &= \frac{1}{L} \phi_{2,\mathbf{k}}(\mathbf{r}) \end{aligned} \quad (14)$$

where the subscript B refers to bulk and S to surface. Note that in this case the hybridization energies between substrate (bulk and surface) and adatom in (8) can be written as:

$$t_{\mathbf{k},a,\alpha} = (\epsilon_a + \epsilon(\mathbf{k})) \frac{1}{L^{d/2}} V_{\alpha}^{(d)}(\mathbf{k}) \quad (15)$$

where $d = 3$ for bulk and $d = 2$ for surface. The matrix elements are, therefore,

$$V_{\alpha}^{(d)}(\mathbf{k}) = \int d^3r \phi_{d,\mathbf{k}}(\mathbf{r}) \psi_a(\mathbf{r}). \quad (16)$$

Notice that $V_{\alpha}^{(d)}(\mathbf{k})$ is not only a function of the momentum and the distance z_0 between adatom and surface, but also depends on which surface - here labeled by the subscript α - the adatom is located.

In Fig. 5 we show the result for $V_{(111)}^{(2)}$, the hybridization matrix element between $m = 0$ adatom state and surface state in the Cu(111) surface, as obtained by numerical integration of (16) using (A1) and (11), as a function of z_0 (in units of the distance between the planes in the (111) direction) by assuming \mathbf{k} to be at the Fermi surface of the surface band [since the surface states have essentially a spherical Fermi surface there is no dependence of $V_{(111)}^{(2)}$ with the direction on the Cu(111) surface]. The first striking result is the strong oscillation of the value of the matrix element with z_0 . This oscillation is the result of the interference between the d-state of the adatom and the surface state. Naturally, the largest overlap occurs at the surface (where the surface state is maximum, see Fig. 4) but we notice that there is substantial overlap between the surface state and the adatom at one lattice spacing from the surface. In principle, we cannot tell what is the actual orientation of the adatom relative to the surface but we have checked that the $m = 0$ state is the one with biggest overlap as compared with higher angular momentum states, thus, instead of a sum over the angular momentum states in Eq.(1) we could have kept only the one with $m = 0$. Furthermore, first principle calculations for adatoms in metallic surfaces indicate that the atomic orbitals are oriented in such a way to generate the largest overlaps²⁵.

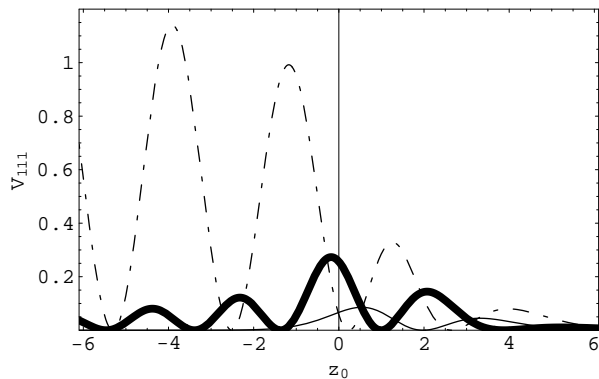


Figure 5: $V_{111}^{(2)}$: dashed-dotted line, $V_{111}^{(3)}(\Gamma-K)$: thick line, and $V_{111}^{(3)}(\Gamma-X)$: thin line, as a function of z_0 .

In Fig. 5 we also plot the value of $V_{(111)}^{(3)}$, the hybridization matrix element between the bulk states and adatom in the Cu(111) surface as a function of the distance from the surface for two different bulk states, all of them at the Cu Fermi surface, with momenta along the $\Gamma-X$, and $\Gamma-K$ directions (see Fig. 2). Once again we notice the oscillations due to the interference between those states and the adatom states but we also observe that the overlap now is a factor of 3 smaller because these states do not have a large amplitude at the surface. Another interesting result of these calculations is the fact that as the momenta moves towards the (111) direction the overlap grows. This is due to the fact that away from the (111) direction the Fermi surface of Cu is essentially spherical and therefore the states at the Fermi surface have essentially the same amplitude, however, the states with large momentum along the direction of the Cu(111) surface have bigger penetration on the potential barrier generated by the work function and therefore larger hybridization with the adatom. This effect will be very important later for the interpretation of the experimental data.

In Fig. 6 we show the value of $V_{(100)}^{(3)}$ for the overlap between the state of an adatom on the Cu(100) surface with bulk states with momenta along the $\Gamma-X$ (this direction is perpendicular to the Cu(100) surface), and $\Gamma-K$ (since there are no surface states for the Cu(100) surface we do not need to calculate $V^{(2)}$ for this surface). Besides the oscillations found in the previous calculations, we find that when the momentum is oriented perpendicular to the surface its penetration is maximum and therefore has largest overlap. In fact, we find that the overlap between the adatom state on a Cu(111) surface with the surface state is essentially the same value as the overlap between the state of the adatom on the Cu(100) surface with a bulk state with momentum oriented in the (100) direction. One can easily understand this effect from the nearly free electron picture: in the absence of the periodic potential of the crystal, the Fermi surface states in the (111) and (100) direction would be essen-

tially identical and their decay in the vacuum of their respective surfaces would be the same. When the periodic potential of the crystal is added a gap opens in the (111) direction but not on the (100) direction. However, the bulk state that disappeared at the Fermi surface in the (111) direction now becomes the surface state in this same surface. Therefore, its amplitude at the surface and close to it is essentially the same as the state in the (100) direction (this can be readily understood due to the long decay rate of the surface state shown in Fig. 4) and the overlap is essentially the same. Thus, one has to be careful when discussing what happens to adatoms in different surfaces because there is very little difference between surface states along gaped directions and bulk states along non-gaped directions in the Fermi surface of noble metals.

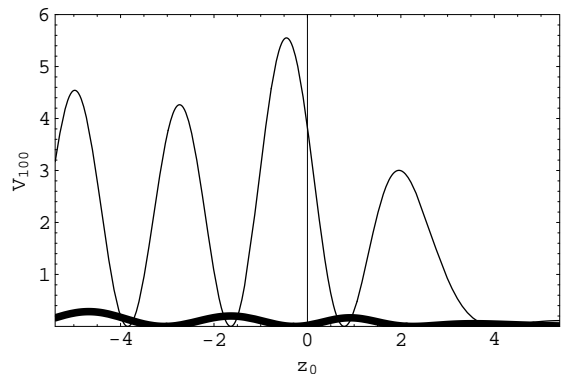


Figure 6: $V_{100}^{(3)}(\Gamma-X)$: thin line, $V_{100}^{(3)}(\Gamma-K)$: thick line, as a function of z_0 .

IV. THE SURFACE KONDO EFFECT

There are two main limits of interest in the Kondo problem. The first one is reached when $|t_{\mathbf{k}a}| \ll |\epsilon_a|, U$ and we can treat the hybridization energy as the smallest scale in the problem. This is the so-called Kondo regime where the average occupation of the impurity state is essentially constant, that is, $\langle n_a \rangle \approx 1$. In order to study this limit it is convenient to split the electron states into bulk (B) and surface (S) so that we write the Anderson impurity Hamiltonian (1) as:

$$\begin{aligned}
 H = & \sum_{\mathbf{k}, \sigma} \epsilon_1(\mathbf{k}) c_{1, \mathbf{k} \sigma}^\dagger c_{1, \mathbf{k} \sigma} + \sum_{\mathbf{q} \sigma} \epsilon_2(\mathbf{q}) c_{2, \mathbf{q} \sigma}^\dagger c_{2, \mathbf{q} \sigma} \\
 & + \epsilon_a \sum_{\sigma} d_{\sigma}^\dagger d_{\sigma} + U n_{a, \uparrow} n_{a, \downarrow} \\
 & + \sum_{\mathbf{k}, \sigma} t_{B, \mathbf{k}a} \left(c_{1, \mathbf{k} \sigma}^\dagger d_{\sigma} + h.c. \right) \\
 & + \sum_{\mathbf{q}a} t_{S, \mathbf{q}a} \left(c_{2, \mathbf{q} \sigma}^\dagger d_{\sigma} + h.c. \right)
 \end{aligned} \tag{17}$$

where $c_{1,\mathbf{k}\sigma}$ ($c_{2,\mathbf{q}\sigma}$) describes the bulk (surface) electron annihilation operator, respectively. We have a two-band problem where both bulk and surface states hybridize with the impurity at the surface. Notice that this is a single channel problem since only one effective channel couples to the impurity.

In the Kondo limit we can use a Schrieffer-Wolf transformation¹⁵ and rewrite the Anderson impurity Hamiltonian as a exchange problem:

$$H = \sum_{\mathbf{k},\sigma,n=1,2} \epsilon_n(\mathbf{k}) c_{n,\mathbf{k}\sigma}^\dagger c_{n,\mathbf{k}\sigma} + \sum_{\mathbf{k},\mathbf{k}'} \sum_{\alpha,\beta=\uparrow,\downarrow} \sum_{n,m=1,2} \mathbf{S} \cdot \vec{\sigma}_{\alpha,\beta} c_{n,\mathbf{k},\alpha}^\dagger J_{n,m}(\mathbf{k},\mathbf{k}') c_{n,\mathbf{k}',\beta} \quad (18)$$

where \mathbf{S} is the localized impurity spin and

$$J_{n,m}(\mathbf{k},\mathbf{k}') = \frac{1}{L^{(d_n+d_m)/2}} \frac{V^{(d_n)}(\mathbf{k}) V^{(d_m)}(\mathbf{k}')}{\lambda} \quad (19)$$

is the exchange energy matrix (we have defined $d_1 = 3$ and $d_2 = 2$ as the dimensionalities of bulk and surface states, respectively), and

$$\frac{1}{\lambda} = \frac{1}{|\epsilon_a|} + \frac{1}{|\epsilon_a + U|}. \quad (20)$$

Notice that, unlike the single band Kondo effect (3), electrons from one band can scatter from the impurity between two different bands with spin flip (all energies are measured relative to the Fermi energy). If we ignore the off-diagonal matrix elements of (19) the problem trivially reduces to two independent Kondo effects with characteristic Kondo temperatures

$$T_{K,n} \approx D_n e^{-1/g_n} \quad (21)$$

where D_n is the bandwidth cut-off ($D_1 \approx 8.6$ eV, $D_2 \approx 0.4$ eV¹⁷) and

$$g_n = N_n(0) J_{n,n}(k_F, k_F) = \frac{1}{L^{d_n}} \frac{N_n(0) |V^{(d_n)}(k_F)|^2}{\lambda} \quad (22)$$

is the effective coupling constant, $N_n(0)$ is the Fermi surface density of states (for spherical Fermi surface we have $N_n(0) = (L/\pi)^{d_n} 2\pi m^* k_F^{d_n-2} / \hbar^2$ where m^* is the effective mass). Because of the difference in the Kondo temperatures given in (21) one of the scattering channels dominates the screening process and the singlet state can be either formed with the surface state when $T_{K,2} > T_{K,1}$ or with the bulk states if $T_{K,1} > T_{K,2}$. If we apply this argument to the results of the overlap integrals of the previous section we see that for the adatom in the Cu(111) surface the Kondo screening is dominated by the surface state since the coupling constant (22) is bigger for this state than the bulk states. On the other hand, if the adatom is sitting at the Cu(100) surface, the Kondo effect is dominated by the bulk state with momentum perpendicular to the Cu(100) surface.

The above discussion is valid as far as the occupation of the impurity level is close to 1. However, in the problem at hand the adatom occupation can change substantially with the hybridization since the matrix element is strongly dependent of the distance to the surface and the type of states involved, that is, $t_{\mathbf{k}a}$ can be of the order of ϵ_a (but still much smaller than U). In this case, the mapping into the Kondo problem fails to properly describe the actual occupation on the adatom. Instead, we should start from the Anderson impurity Hamiltonian (1) and compute the Kondo temperature directly from it. Here we will do so by adopting the large N calculation of Newns and Read²⁶ that allows for average fluctuations in the valence of the adatom in the limit of $U \rightarrow \infty$ (in fact, estimates based on LSDA¹⁹ give a value of $U \approx 2.84$ eV and $\epsilon_a \approx -0.84$ eV). The idea of the large N calculation is to generalize (1) to include more degenerate electron states (besides the 2 states associated with the spin 1/2) and take the limit where the degeneracy diverges. Mathematically this is accomplished by generalizing the spin index in the electron operator to a new index m that varies from 1 to N . It is convenient to write Anderson impurity Hamiltonian (1) in the limit of $U \rightarrow \infty$ as:

$$H_s = \epsilon_a \sum_m c_{a,m}^\dagger c_{a,m} + \sum_{\mathbf{k},m} \epsilon_{\mathbf{k}} c_{\mathbf{k},m}^\dagger c_{\mathbf{k},m} + \sum_{\mathbf{k},m} t_{\mathbf{k},a} \left(c_{\mathbf{k},m}^\dagger c_{am} \mathcal{P} + \text{H.c.} \right) \quad (23)$$

where \mathcal{P} is the projector operator that projects out any states of the adatom with double occupancy. In the adatom we can, in principle, have three different states with zero, $|d^0\rangle$, single, $|d^1\rangle$, and double, $|d^2\rangle$, occupancy. We now expand the Hilbert space by introducing a “phantom” boson state such that when the state of the adatom is unoccupied by an electron it is occupied by a boson, say $|b^1 d^0\rangle$, and when it is unoccupied by a boson it is occupied by an electron, $|b^0 d^1\rangle$. Observe that this construction constrains the number of bosons and electrons to be 1 for all states $|\psi\rangle$ in the Hilbert state:

$$(n_a + b^\dagger b) |\psi\rangle = 1 |\psi\rangle. \quad (24)$$

The utility of this representation becomes clear when we consider the action of the operator $c_{am}^\dagger b$ on the state $|b^1 d^0\rangle$ producing the state $|b^0 d^1\rangle$. Further application of $c_{am}^\dagger b$ to $|b^0 d^1\rangle$ annihilates the state while application of $c_{am} b^\dagger$ to $|b^0 d^1\rangle$ returns the system to the state $|b^1 d^0\rangle$. Thus, the repetitive application of $c_{am}^\dagger b$ or $c_{am} b^\dagger$ never produces the doubly occupied state. In other words, we can replace \mathcal{P} in (23) by a boson operator if we ensure that the constraint (24) is obeyed. This constraint can be seen as an energy cost, that is, states of the Hamiltonian that violate the constraint (24) are highly excited states. If we are interested in the low energy physics then we can convert (24) into a new energy scale and add it to

the Hamiltonian as:

$$\begin{aligned}
H_s = & \epsilon_a \sum_m c_{a,m}^\dagger c_{a,m} + \sum_{\mathbf{k},m} \epsilon_k c_{\mathbf{k},m}^\dagger c_{\mathbf{k},m} \\
& + \sum_{\mathbf{k},m} t_{\mathbf{k},a} \left(c_{\mathbf{k},m}^\dagger c_{am} b + \text{H.c.} \right) \\
& + \gamma (n_a + b^\dagger b - 1)
\end{aligned} \quad (25)$$

where γ is a Lagrange multiplier. Notice that in the limit of $\gamma \rightarrow \infty$ the constraint (24) is automatically obeyed since the energy is minimized when (24) is fulfilled. As is, Hamiltonian (25) is still very complicated and at this point we have to use the large N approximation that consists in treating (25) in a mean-field approximation. In the mean-field limit we consider the average value of the boson fields instead of their actual value, that is, we replace the operators b and b^\dagger by

$$\langle b \rangle = \langle b^\dagger \rangle = \sqrt{z}. \quad (26)$$

Notice that by treating the bosons in the mean-field approximation we obtain a quadratic Hamiltonian in (25) that can be diagonalized by standard techniques and the total energy of the system can be minimized with respect to z and γ . The physical meaning of these parameters becomes clear when we calculate physical observables. For instance, the average occupation of the impurity is given by:

$$\langle n_a \rangle = 1 - z \quad (27)$$

that shows that z has to do with the change in the occupancy of the adatom state due to the hybridization with the substrate. On the other hand we can also show that γ is the renormalization of the energy of the impurity state, that is, the renormalized impurity state energy is given by: $\bar{\epsilon}_a = \epsilon_a + \gamma$. The mean-field parameters $\bar{\epsilon}_a$ and z are calculated by solving a set of coupled transcendental equations²⁶:

$$\begin{aligned}
1 - z &= \frac{2}{\pi} \arctan \left(\frac{z F_{aka}(\epsilon_F)}{|\bar{\epsilon}_a|} \right), \\
\epsilon_a - \bar{\epsilon}_a &= \frac{2}{\pi} F_{aka}(\epsilon_F) \ln \left(\frac{\left\{ \bar{\epsilon}_a^2 + [z F_{aka}(\epsilon_F)]^2 \right\}^{1/2}}{D} \right)
\end{aligned} \quad (28)$$

where $F_{ak\beta}(\omega)$ are matrices defined, in general, as:

$$F_{ak\beta}(\omega) = \sum_{\mathbf{k}} \frac{t_{\alpha\mathbf{k}} t_{\mathbf{k}\beta}}{\omega - \epsilon_{\mathbf{k}} + i\eta}, \quad (29)$$

and D is bandwidth of the conduction band (notice that $\alpha, \beta = a, p$ in reference to the adatom and tip, respectively). The Kondo temperature can be directly extracted from this formalism as²⁶

$$k_B T_K = z \Delta_0 = D \exp \left(\frac{\pi \epsilon_a}{\Delta_0} \right). \quad (30)$$

where

$$\Delta_0 = \text{Im } F_{aka}(\omega). \quad (31)$$

Therefore, using the large N account we can deal with the case where the hybridization energies are of the order of the adatom energies. We use these results in studying the STM differential conductance in the next section.

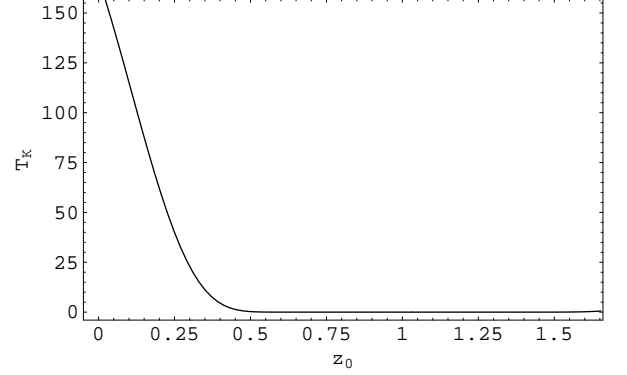


Figure 7: Kondo temperatures as functions of the Co distance from the surface, z_0 , on the Cu(111) surface.

We are not aware of any measurement of Co-to-Cu distance being reported, so this distance z_0 will be treated as a parameter of the order of the Cu lattice space. Fig. 7 and 8 shows our calculated Kondo temperature as a function of z_0 . An interesting feature is that the Kondo temperature decays fast with z_0 , which can be understood because of the exponential overlap between the substrate and Co wavefunctions. When calculating the Kondo temperature for Co/Cu(111) assuming that only the bulk state exists, we find $T_K < 10^{-6} K$ for the z_0 's as Fig. 7, which clearly means that the surface state dominates the Kondo effect. The domination is not surprising since a significant portion of large- k_\perp bulk states are gaped around the (111) direction. Comparing the Cu Fermi surface with a perfectly spherical one, one finds that the Cu surface state contributes to the Kondo effect in a way similar to the bulk band of the spherical Fermi surface around the (111) direction. Similarly, the bulk band with respect to the Cu(100) surface can be considered as a perfectly spherical Fermi surface for calculating the Kondo effect. As a result, the Kondo effect of the Co/Cu(111), dominated by the surface state, should have the same order of magnitude as Co/Cu(100). The positions that provide the experimentally measured Kondo temperatures²⁷ ($T_{K,(111)} = 54 K$ and $T_{K,(100)} = 88 K$) are 0.41 Å and 0 from the (111) and (100) surfaces, respectively. Hence the STM conductance will be calculated by fixing Co atom at these optimized positions.

We should point out that from an experimental point of view we would expect the Co adatom to be located around one lattice spacing away from the surface. Thus, our obtained values of their position seem to be quite

small (especially in the case of the (100) surface where the adatom has to be located at the surface) and therefore unrealistic. Nevertheless, one has to have in mind that there are many assumptions made in the calculation that can affect significantly the value of the Kondo temperature, namely, the form of the image potential close to the surface, the large N approximation, and the limit of $U \rightarrow \infty$. Furthermore, it is clear from (30), that the Kondo temperature is exponentially sensitive on the details of the hybridization and energy scales and therefore is significantly affected by the various assumptions. Thus, the plots in Fig.7 and Fig.8 have to be taken as the trends for the variation of the Kondo temperature with the distance from the surface and not as realistic values.

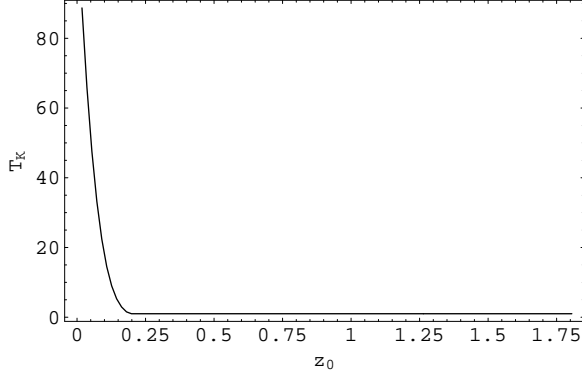


Figure 8: Kondo temperature as functions of the Co distance, z_0 , on the Cu(100) surface.

V. STM DIFFERENTIAL CONDUCTANCE

We assume that the STM tip and the adsorbate-substrate complex are each in local equilibrium, and use the standard Green's function formalism for calculation of the differential conductance¹¹:

$$\frac{dI}{dV} \propto -\text{Im} \left\{ F_{pkip}(\omega) + G_a(\omega) [t_{pa} + F_{pka}(\omega)]^2 \right\}_{\omega=eV}, \quad (32)$$

where $F_{\alpha k \beta}(\omega)$ is defined in (29) and G_a is formally the adsorbate retarded Green's function associated with the total Hamiltonian H . However, because the effect on the adsorbate from the tip is much smaller than that from the substrate, it is always safe to regard G_a as the one without tip. In this work, G_a (without tip) is calculated by the mean-field slave-boson technique²⁶ as:

$$G_a(\omega) = \frac{1}{\omega - \bar{\epsilon}_a + iz\Delta_0}, \quad (33)$$

where the symbols here are given in the previous section.

By substituting (33) into (32), the STM differential conductance can be written as:

$$\frac{dI}{dV} - \left(\frac{dI}{dV} \right)_0 = A \left[\frac{q^2 - 1 + 2q\xi}{\xi^2 + 1} \right], \quad (34)$$

where the differential conductance with a subscript “0” refers to the background signal, A is the amplitude of the STM conductance,

$$A \propto (\text{Im} F_{pka})^2 (1 + q^2), \quad (35)$$

q is the Fano lineshape parameter,

$$q = \frac{t_{pa} + \text{Re} F_{pka}(\omega)}{\text{Im} F_{pka}(\omega)}, \quad (36)$$

and ξ is the dimensionless bias voltage

$$\xi = \frac{eV + \bar{\epsilon}_a}{k_B T_K}. \quad (37)$$

Expression (34) has been frequently used for the fitting of STM data.

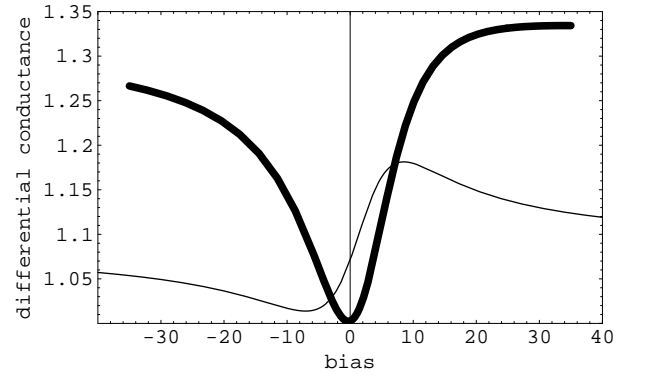


Figure 9: Differential conductance (in arbitrary units) at $R_{\parallel} = 0$, as a function of the bias V in meV for an adatom on the Cu(111) (thick line) and Cu(100) (thin line) surfaces, as obtained from the theoretical calculations.

The shape of the differential conductance versus the bias voltage is determined by the Fano line shape parameter q . In Fig.9 we show the differential conductances obtained from our microscopic theory for the Cu(111) and Cu(100) surfaces. From Eq. (36) we see that q is related to three microscopic quantities t_{pa} , $\text{Im} F_{pka}(\omega)$, and $\text{Re} F_{pka}(\omega)$. It is found that $t_{pa} \ll \text{Re} F_{pka}(\omega)$ and therefore we can set $t_{pa} = 0$ in (36). Obtaining the first two is straightforward since they only depend on the physics at the Fermi energy. From (29), we have:

$$\text{Im} F_{\alpha k \beta}(\omega) = \pi \sum_{\mathbf{k}} t_{\alpha \mathbf{k}} t_{\mathbf{k} \beta} \delta(\omega - \epsilon_{\mathbf{k}}). \quad (38)$$

Notice that the amplitude of the STM signal, (35), depends essentially on this quantity and can be calculated reliably. In Fig.10 we plot $A(R_{\parallel})$ for $R_{\perp} = 6 \text{ \AA}$ and compare it with the experimental data²⁷. As one can see, the agreement between the theory and experiment and theory is quite good.

The other quantity of interest, namely, $\text{Re} F_{pka}(\omega)$, requires an integration over the entire Cu band. For the

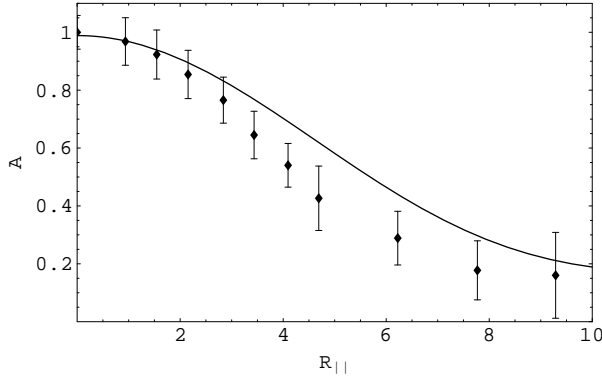


Figure 10: Amplitude of the differential conductance (in arbitrary units) for Co on Cu(111) as a function of R_{\parallel} as compared with the experimental data²⁷.

Cu(111) surface, the surface band has a free-electron dispersion starting 390 meV below the Fermi level up to 400 meV above it, where the upper limit is the intercept of the surface band to the bulk bands. We calculate $\text{Re } F_{pka}(\omega)$ for this surface band and determine the tunneling conductances, (34), for different values of R_{\parallel} as shown in shown in Fig. 11.

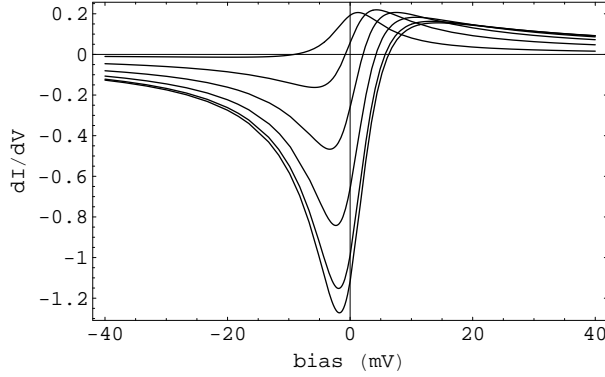


Figure 11: Differential conductances for the Co on Cu(111) for different values of R_{\parallel} . From bottom to the top: $R_{\parallel} = 0, 2, 4, 6, 8, 10 \text{ \AA}$

We notice that for short distances away from the adatom, the theory can describe very well the lineshape of the tunneling conductance. Nevertheless, as the distance of the STM tip to the adatom is increased, the lineshape becomes more symmetric and a positive Lorentzian is developed (see Fig.11). The origin of this result can be easily understood: notice that in Fig.10 the amplitude of the STM conductance becomes very small for large values of R_{\parallel} . This smallness can be tracked down to the small value of $\text{Im } F_{pka}$ in (35) indicating that the interference between tip and adatom is fading away. However, one sees from (36) that this indicates that the Fano parameter q is becoming very large and positive given rise

to a positive Lorentzian. This feature is general of any theory of the STM conductance that starts with nearly free electron wavefunctions and cannot be avoided since it has its origins on the oscillating nature of the surface states density of states¹¹. This result is at odds with the experiment when the distance between tip and adatom becomes large. Instead of a positive Lorentzian, it is observed a negative Lorentzian²⁸.

In Fig.12 we plot the calculated values of q against the values used by the experimentalists in order to fit the data²⁷. The discrepancy between theory and experiment is clear. More work will be required in order to check this issue.

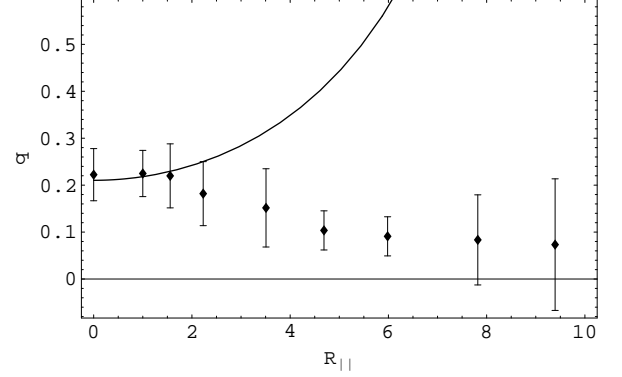


Figure 12: Plot of the Fano parameter $q(R_{\parallel})$ for Co on Cu(111) as compared with the values obtained by the experimental fit²⁷.

In order to calculate $\text{Re } F_{pka}(\omega)$ for an adatom located at the Cu(100) surface we need information of the whole Cu bulk band. The Cu bulk bands start at approximately 10 eV below the Fermi level and disperse up to the vacuum level that is located at approximately at 4.8 eV above the Fermi energy. At the Fermi energy the Cu band has dominant s-wave symmetry which gives the quasi-spherical shape of the Fermi sea. However, there are also Cu d-bands located from 2 to 5.5 eV below the Fermi level with very large density of states¹⁶. Using the nearly free electron approximation (s-wave) with a cut-off at the vacuum level we have calculated $\text{Re } F_{pka}(\omega)$ and have found that it yields a value of $q(R_{\parallel})$ that changes sign from positive to negative as R_{\parallel} increases, which is not the case observed in the experiment. In principle the quantity $\text{Re } F_{pka}(\omega)$ must be calculated including the d-bands. Using a simple parabolic dispersion for the d-bands we find their contribution to be less than 0.1% of the total value of $\text{Re } F_{pka}(\omega)$ and therefore these bands are not able to fix the problem of the sign of $q(R_{\parallel})$. Thus, we have problems with the use of bulk states in our calculation. We believe that band structure effects are important for the exact calculation of the surface Kondo effect due to bulk states. As far as we know there are no such detailed calculations.

In order to remedy this problem we introduce a cut-off in the problem such that by integrating bulk states

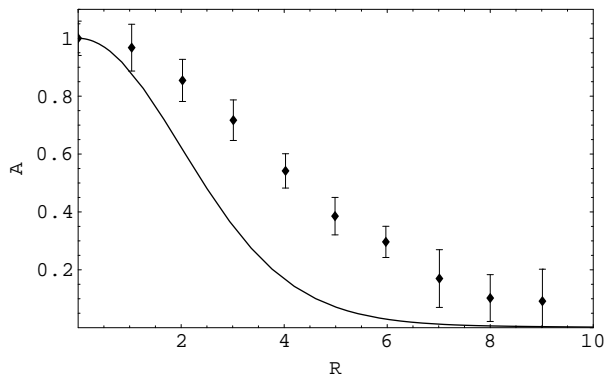


Figure 13: Amplitude of the differential conductance (in arbitrary units) for Co on Cu(100) as a function of R_{\parallel} as compared with the experimental data²⁷.

starting from the bottom of the nearly free electron band we stop the integration when the value of $\text{Re } F_{pka}(\omega)$ fits the experimental curve at $R_{\parallel} = 0$. We find that if we integrate up to 0.25 eV above the Fermi level we can quantitatively explain the data, as seen in Fig. 9. Given the limitations of our theory this is essentially equivalent to consider $\text{Re } F_{pka}(\omega)$ for adatom on the Cu(100) surface for bulk states as a free parameter of the problem. More accurate calculations, beyond the ones presented in this paper, are required in order to calculate $\text{Re } F_{pka}(\omega)$ from a microscopic theory.

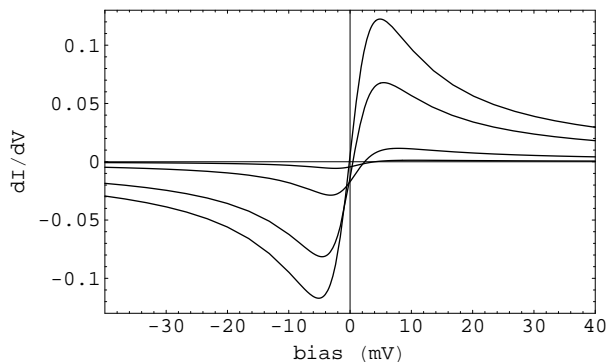


Figure 14: Differential conductances for the Co on Cu(100) for different values of R_{\parallel} . From bottom to the top: $R_{\parallel} = 0, 2, 4, 6$ Å

In Fig. 13 we show the amplitude $A(R_{\parallel})$ for Co on Cu(100) for $R_{\perp} = 9$ Å. There is a qualitative agreement between theory and the experiment. In Fig. 14 we show the evolution of the tunneling conductance as a function of the distance from the adatom. Once again, the lineshape is correct for short distances but for long distances the lineshape becomes a positive lorentzian, in contrast with the experiment. In fact, in Fig. 15 we show the dependence of the Fano parameter, q , as a function of the

lateral distance, R_{\parallel} . Notice that overall result is better than the case of Co on Cu(111) (Fig. 12) but the divergence in the value of q is very clear.

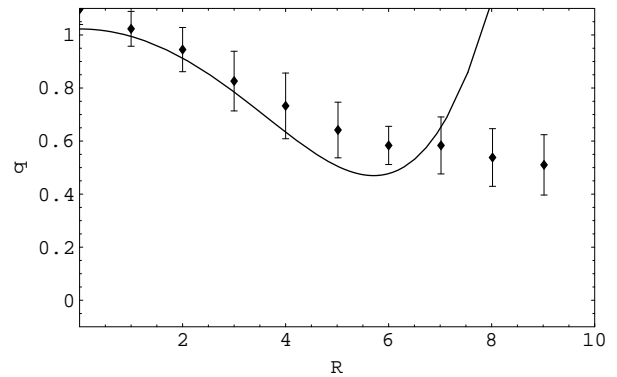


Figure 15: Plot of the Fano parameter $q(R_{\parallel})$ for Co on Cu(100) as compared with the values obtained by the experimental fit²⁷.

VI. CONCLUSIONS

In this paper we have studied the microscopic theory of the single impurity surface Kondo resonance starting from an Anderson impurity Hamiltonian. We have calculated the hybridization energies and wavefunctions of the model adopting simple models for the crystal and surface potentials in the nearly-free electron approximation. Our model reproduces the main features of the band structure of Cu, the energy of the surface states and surface resonances as measured in photoemission experiments.

We have shown that the hybridization energies (or matrix elements), calculated from the solution of the single particle Schrödinger equation, are strongly dependent on the direction of the electron momenta, the distance of the adatom from the surface, and the actual surface where the magnetic impurity is located. The hybridization matrix elements oscillate with distance from the surface due to the interference between the adatom localized state and the substrate states (surface and bulk) that oscillate close to the surface. We have shown that the surface Kondo effect occurs preferentially with the surface state (when it exists) or with the bulk state at the Fermi energy that has the largest component of its momentum perpendicular to the surface.

We have demonstrated that although the surface Kondo effect can be obtained from the Anderson impurity Hamiltonian by a Schrieffer-Wolf transformation onto the Kondo Hamiltonian, the hybridization energies can be comparable with the adatom atomic energy requiring a more sophisticated approach that allows for fluctuations in the mean occupation of the adatom (in other words, the adatom is in what is called a mixed-valence state). We have used the mean-field slave-boson

formalism that allows for the calculation of the Kondo temperature in the limit when the on-site Coulomb energy U is much larger than the hybridization energy. Our results produce reasonable values of the Kondo temperature for these systems and the distance of the adatom from the surface.

We have calculated the tunneling conductance of a STM tip for different surfaces in the presence of a Co impurity and found that for the surface state in the Cu(111) surface we get quantitative agreement without any further adjustable parameters. However, for the adatom on the Cu(100) surface where the Kondo effect is dominated by the bulk state with momentum along the (100) direction, we have to add an extra cut-off energy in order to fit the data. More detailed band structure calculations are required in order to eliminate the need for this extra parameter. We have shown that in both cases we can fit very well the data obtained in STM measurements at $R_{||} = 0$ but there is a discrepancy between the theory and experiments when the distance between the tip and the adatom becomes large. While in the experimental paper where the measurements are reported it is conjectured that the Kondo effect in the Cu(111) and Cu(100) surfaces are dominated by the bulk states²⁷, we show that in fact, the Kondo effect is dominated by the surface state in the Cu(111) surface and by the bulk state with momentum in the (100) direction in the (100) surface. We show that this occurs because there is very little difference between surface states and bulk states close to the surface in a noble metal and both states have maximum penetration on the work function potential.

In summary, we provide a microscopic interpretation for the STM experiments of surface Kondo effects. Our results can be used as basis for the interpretation of more complicated situations where, for instance, Co adatoms interact via direct or indirect exchange on artificial Anderson lattices in metallic surfaces.

Acknowledgments We would like to thank I. Affleck, P. W. Anderson, A. Balatsky, P. Coleman, D. Eigler, A. Heinrich, P. Johnson, C. Lutz, V. Madhavan, P. Simon, and A. Tsvelik, for illuminating discussions. We

also would like to acknowledge support under DARPA contract no. DAAD19-01-C-0060.

Appendix A: EXPLICIT COPPER WAVEFUNCTIONS

For the Cu(111) surface state, the parallel momentum $\mathbf{k}_{||}$ is a good quantum number, and the wavefunction can be solved from potential Eq. (9) as:

$$\psi(\mathbf{r}) = e^{i\mathbf{k}_{||} \cdot \mathbf{r}_{||}} \times \begin{cases} e^{\mu z} \cos(k_z z + \delta), & \text{for } z < 0, \\ \mathcal{A} \cos \lambda z + \mathcal{B} \sin \lambda z, & \text{for } 0 < z < z_1, \\ C z' e^{-\kappa z'} U\left(1 - \frac{a}{4\pi a_0 \kappa}, 2; 2\kappa z'\right), & \text{for } z > z_1. \end{cases} \quad (\text{A1})$$

where $U(a, b; x)$ is the standard 2nd solution of confluent hypergeometric equation²⁹, $z' = z - z_{\text{im}}$, and $k_z = \pi/2$. Inside the crystal one has a phase shift δ , a crystal decay factor μ , and the energy of the surface band bottom E related by

$$V_1 \cos 2\delta = -\frac{V_1^2 m a^2}{2\hbar^2 \pi^2} \sin^2 2\delta + \frac{\hbar^2 \pi^2}{2m a^2} - E, \\ \frac{\hbar^2 \mu^2}{2m} = \left(V_1^2 + \frac{2\hbar^2 \pi^2}{m a^2} E\right)^{1/2} - \left(\frac{\hbar^2 \pi^2}{2m a^2} + E\right) \quad (\text{A2})$$

where $m = 0.84m_e$ is the bulk-band effective mass. The plane wavefunction has a wavevector

$$\lambda = \frac{1}{\hbar} [2m(E + 2V_1)]^{1/2}, \quad (\text{A3})$$

while vacuum decay factor κ is defined as

$$\kappa = \frac{1}{\hbar} [2m(V_0 - E)]^{1/2}. \quad (\text{A4})$$

The energy E is obtained from the continuity conditions at $z = 0$ and $z = z_1$.

¹ J. Kondo, Prog. Theor. Phys. (Kyoto), **32**, 39 (1964).

² K. G. Wilson, Rev. Mod. Phys. **47**, 773 (1975).

³ N. Andrei, K. Furuya, and J. Lowenstein, Rev. Mod. Phys. **55**, 331 (1983).

⁴ See, for instance, G. R. Stewart, Rev. Mod. Phys. **56**, 755 (1984), and references therein.

⁵ S. Sasaki, S. de Francheschi, J. M. Elzerman, W. G. van der Wiel, M. Eto, S. Tarecha, and L. P. Kouwenhoven, Nature **405**, 764 (2000).

⁶ P. Monod, Phys. Rev. Lett. **19**, 1113 (1967).

⁷ H. Suhl, Phys. Rev. **138**, A515 (1965); A. A. Abrikosov, Physics **1**, 5 (1965).

⁸ Jintao Li, W.-D. Schneider, R. Berndt, and B. Delley, Phys. Rev. Lett. **80**, 2893 (1998).

⁹ V. Madhavan, W. Chen, T. Jamneala, M. F. Crommie,

and N. S. Wingreen, Science **280**, 567 (1998).

¹⁰ H. C. Manoharan, C. P. Lutz, and D. M. Eigler, Nature (London) **403**, 512 (2000).

¹¹ M. Plihal and J. W. Gadzuk, Phys. Rev. B **63**, 085404 (2001).

¹² P. W. Anderson, Phys. Rev. **124**, 41 (1961).

¹³ As pointed out in ref.¹⁴, the radius of the d-orbital, r_B , is much smaller than the average interparticle distance, k_F^{-1} (where k_F is the Fermi momentum): $k_F r_B \ll 1$. Hence, the corresponding overlap integrals between the adatom and the substrate are small.

¹⁴ A. M. Tsvelik, and P. B. Wiegmann, Adv. Phys. **32**, 453 (1983).

¹⁵ J. R. Schrieffer and P. A. Wolff, Phys. Rev. **149**, 491 (1966).

- ¹⁶ G. A. Burdick, Phys. Rev. **129**, 138 (1963).
- ¹⁷ J. A. Knapp, F. J. Himpsel, and D. E. Eastman, Phys. Rev. B **19**, 4952 (1979).
- ¹⁸ *Basic Theory of Surface States* by S. G. Davison and M. Steslicka (Oxford University Press, 1996).
- ¹⁹ O. Úsághy, J. Kroha, L. Szunyogh, and A. Zawadowski, Phys. Rev. Lett. **85**, 2557 (2000).
- ²⁰ S. D. Kevan, Phys. Rev. Lett. **50**, 526 (1983).
- ²¹ K. Giesen, F. Hage, F. J. Himpsel, H. J. Riess, and W. Steinman, Phys. Rev. Lett. **55**, 300 (1985).
- ²² N. V. Smith, Phys. Rev. B **32**, 3549 (1985).
- ²³ D. P. Woodruff, S. L. Hulbert, P. D. Johnson and N. V. Smith, Phys. Rev. B **31**, 4046 (1985).
- ²⁴ J. Tersoff and D. R. Hamman, Phys. Rev. B **31**, 805 (1985).
- ²⁵ P. Nordlander and J. C. Tully, Phys. Rev. B **42**, 5564 (1990).
- ²⁶ D. M. Newns and N. Read, Adv. Phys. **36**, 799 (1987).
- ²⁷ N. Knorr, M. A. Schneider, L. Diekhoner, P. Wahl, and K. Kern, Phys. Rev. Lett. **88**, 096804 (2002).
- ²⁸ See Fig.1 of ref.¹⁰ for the case of Co on Cu(111), and Fig.3 of ref.⁹ for the case of Co on Au(111).
- ²⁹ G. B. Arfken and H. J. Weber, *Mathematical methods for physicists* (Academic Press, San Diego, 1995).